



OPEN ACCESS

EDITED BY

Mohammad Abdelfattah Sarhan,
Damietta University, Egypt

REVIEWED BY

Haytham Sehsah,
Damietta University, Egypt
Ahmed Shalaby,
Mansoura University, Egypt

*CORRESPONDENCE

Sherif Mansour,
✉ sherif@sci.psu.edu.eg

RECEIVED 25 March 2023

ACCEPTED 21 April 2023

PUBLISHED 04 July 2023

CITATION

Mansour S, Gharib MA, Hasebe N,
Abdelrahman K, Fnais MS and Tamura A
(2023), Tectonic evolution of the Gabal
Loman area, North Eastern Desert, Egypt:
implications from low-temperature
multithermochronometry on the
Arabian-Nubian shield.
Front. Earth Sci. 11:1193692.
doi: 10.3389/feart.2023.1193692

COPYRIGHT

© 2023 Mansour, Gharib, Hasebe,
Abdelrahman, Fnais and Tamura. This is
an open-access article distributed under
the terms of the [Creative Commons
Attribution License \(CC BY\)](https://creativecommons.org/licenses/by/4.0/). The use,
distribution or reproduction in other
forums is permitted, provided the original
author(s) and the copyright owner(s) are
credited and that the original publication
in this journal is cited, in accordance with
accepted academic practice. No use,
distribution or reproduction is permitted
which does not comply with these terms.

Tectonic evolution of the Gabal Loman area, North Eastern Desert, Egypt: implications from low-temperature multithermochronometry on the Arabian-Nubian shield

Sherif Mansour^{1*}, Mohamed A. Gharib¹, Noriko Hasebe²,
Kamal Abdelrahman³, Mohammed S. Fnais³ and Akihiro Tamura⁴

¹Geology Department, Faculty of Science, Port Said University, Port Said, Egypt, ²Institute of Nature and Environmental Technology, Kanazawa University, Kanazawa, Japan, ³Department of Geology & Geophysics, College of Science, King Saud University, Riyadh, Saudi Arabia, ⁴Department of Earth Sciences, Kanazawa University, Kanazawa, Japan

The Neoproterozoic Arabian-Nubian Shield (ANS) in the Eastern Desert of Egypt encloses the regional thermal-tectonic history from its development till the Oligo-Miocene when the Red Sea rift system was initiated. The application of multi-thermochronometry techniques has proven to be a successful approach to revealing the influence and extent of each regional tectonic event and the recreation of the tectono-thermal development of the studied region through time. Therefore, characteristic samples from the ANS different rock suits of the Gabal Loman area at the western flank of the northern Red Sea were collected. The Zircon fission-track data reveals the Carboniferous cooling ages, while the apatite fission-track cooling ages present two differential time spans of Cretaceous and Eocene-Oligocene. The time-temperature history modeling is integrated with fission-track data to reveal three differentiated cooling events developed in response to regional tectonic events: 1) the Hercynian (Variscan) tectonic event that influenced the ANS vicinity with rock uplifts of ca. 4 km through the Devonian-Carboniferous time, 2) the Gondwana disintegration event which influenced the region with differential rock exhumations, and 3) the northern Red Sea rifting through the Oligo-Miocene which caused a regional ca. 1 km of rift flanks exhumation. This modest rift flank uplift suggests a passive rift of the northern Red Sea rifting in the region of study.

KEYWORDS

rift flanks, fission-track, Egypt thermochronology, LA-ICP-MS, Eastern Desert, Arabian-Nubian shield, the Red Sea rifting

1 Introduction

The Red Sea/Gulf of Suez rift system (RSRS) is initiated as part of the deep-seated Afar mantle plume activity, which causes the separation between Africa and Arabia as they previously collided with Eurasia (Bellahsen et al., 2003; Bosworth et al., 2005; Almalki et al., 2015). The RSRS, as a newborn ocean, was always the role model for developing a geodynamic model of continental lithospheric breakup and the subsequent onset of

seafloor spreading (Burke and Dewey, 1973; Sengör and Burke, 1978; Burke, 1996). This is because the extension along the Red Sea Rift has developed into a juvenile oceanic basin, while the Suez Rift extension has slowed down substantially since the middle Miocene, preserving a continental crust beneath it (Boone et al., 2021).

The RSRS is delimited by pronounced rift flanks of the Precambrian basement of the Arabian-Nubian Shield (ANS) exposed in Sinai and the Eastern Desert of Egypt (Figure 1). The ANS is developed during the orogeny of East Africa (EAO; 900–650 Ma) by a collision between East and West Gondwana and the accretion of island arcs and micro-continents into the Sahara Metacraton (Stern, 1994; Meert et al., 2011; Johnson, 2014). The ANS in the North Eastern Desert (NED) consists mainly of syn- to post-tectonic granites (Mansour et al., 2022a; Mansour et al., 2023a) and lesser occurrences of metasedimentary, metavolcanic, and bimodal dykes (Be’eri-Shlevin et al., 2012; El-Bialy, 2020; Mansour et al., 2022a). These rocks have experienced a prolonged tectonic history from the Neoproterozoic, the Precambrian post-accretion erosional event (PAEE), the Devonian-Carboniferous Hercynian tectonic event,

the Cretaceous Gondwana disintegration, and the Oligocene-Miocene northern Red Sea/Gulf of Suez rifting (e.g., Mansour, 2016; Boone et al., 2021).

Reconstructing a temporal-spatial relationship of the rift flank exhumation history, the rift axis tectonic extension and the accompanied magmatism would improve our understanding of the rift evolution and assessment of the possible role of any accompanied thermal overprint (Steckler, 1985; Garfunkel, 1988; Bohannon et al., 1989; Omar and Steckler, 1995; Hansen et al., 2012). Generally, rifts provide the majority of the recoverable hydrocarbon (Morley, 1999); particularly, the RSRS produces approximately 75% of Egypt’s crude Oil (EGPC, 1996). In such geologic settings, tectonics and tectonically shaped topography are key factors that frame the basin stratigraphic sequence that controls the different components of the hydrocarbon system (Lambiase and Morley, 1999). The apatite fission track (AFT) partial annealing zone (PAZ), which is responsible for track accumulation and retention processes occur at temperatures between 60 °C and 120 °C (e.g., Naeser and Faul, 1969; Green et al., 1989). This is almost the typical temperature (between 60 °C and 130 °C) zone

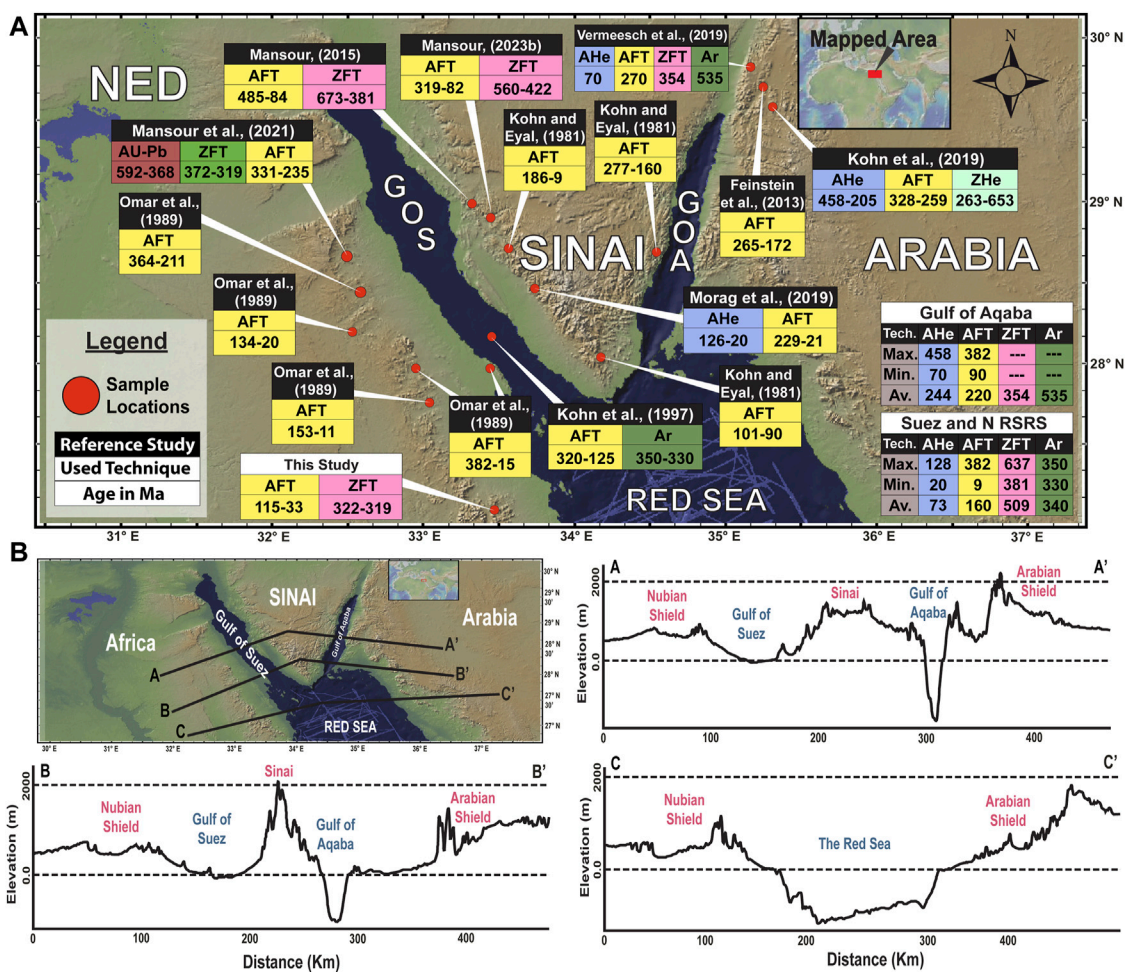


FIGURE 1 (A) The location map for the northern ANS, representing the current study sampling location and the previous thermochronologic studies. Where, ZFT = zircon fission-track, ZHe; zircon (U-Th)/He, Ar = Ar-Ar dating; AFT = apatite fission-track, and AHe; apatite (U-Th)/He. (B) The locations of the represented topographic cross sections (A-A', B-B', C-C') (modified after Mansour et al., 2023b).

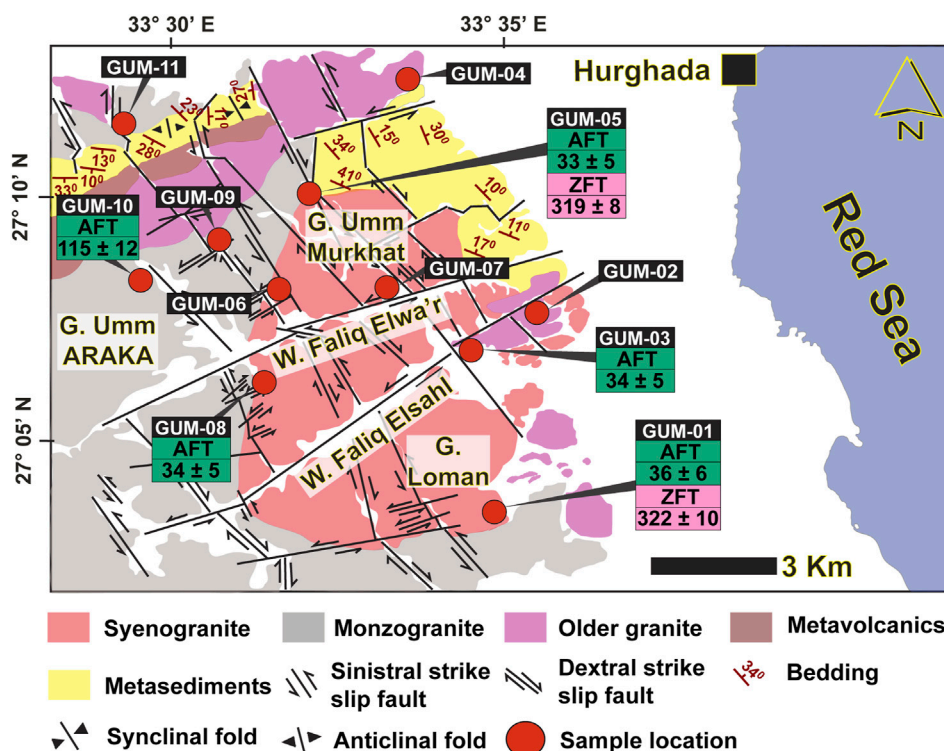


FIGURE 2
The geological and structural map for the G. Loman area (modified after, El-Wakel et al., 2021), representing the studied samples and obtained ZFT and AFT ages.

required for the maturation process of hydrocarbon. Therefore, the AFT technique provides a tool to trace the heating/cooling process, which is the hardest to be predicted among different factors in the hydrocarbon maturation processes (Gleadow et al., 1983).

In this study, we present the apatite (AFT) and zircon (ZFT) fission-track data and time-temperature (t-T) modeling results at the Gabal Loman area on the Red Sea western flank, NED, Egypt (Figure 2). Our data is presented in the context of the previously reported low-temperature thermochronologic data to evaluate the ANS formation and the RSRS development in the region. The integration of different thermochronological techniques has proven to be a beneficial information provider, particularly on the upper crust development through geological times (Batt and Brandon, 2002; Donelick et al., 2005; Reiners and Ehlers, 2005; Lisker et al., 2009).

2 Geologic setting and regional tectonics

The RSRS is developed as part of the tectonic activities in the triple-junction of Afar, which is triggered by the slab-pull effect along the proto-Bitlis-Zagros- Makran convergent zone (Bosworth et al., 2005). This subduction caused compression and rock exhumations of the northern Arabian Margin ca. 50 Ma (Mount et al., 1998; Grobe et al., 2019; Boone et al., 2021). The first voluminous East African Superplume-related basalt eruption

occurred across northern Kenya and southern Ethiopia ca. 45 Ma (Ebinger and Sleep, 1998; George et al., 1998; Rooney, 2017). The Africa-Arabia rifting started by ca. 34 Ma in the eastern proto-Gulf of Aden (Leroy et al., 2012; Pik et al., 2013; Serra-Kiel et al., 2016). This was synchronous with the onset of the Red Sea rifting along the Egyptian margin (Omar and Steckler, 1995). The second voluminous plume-related flood basalts erupted between 31 Ma and 29 Ma in the Afar region across Ethiopia, northeast Sudan, and southwest Yemen (Hofmann et al., 1997; Bosworth and Stockli, 2016). Furthermore, widespread volcanic centers were activated to form the Older Harrats through the margin of western Arabia between 30–20 Ma (Bosworth and Stockli, 2016). During the Older Harrats eruptions, limited volcanisms and normal faulting were developed along the Eritrean-Yemeni border at ca. 28–20 Ma (Hughes et al., 1991; Menzies et al., 1997; Ghebreab et al., 2002; Balestrieri et al., 2009; Bosworth and Stockli, 2016), while the African margin of the Gulf of Aden remained volcanically active until ca. 16 Ma (Leroy et al., 2010; 2012; Ahmed et al., 2013; Corbeau et al., 2014; Nonn et al., 2019). A major extensional period during ca. 25 Ma is recorded in the Afar and Jizan Basins through the south margin of Arabia (Cole et al., 1995; Stab et al., 2016). Between 24 Ma and 21 Ma, extensive magmatic intrusions, diking, and volcanisms that are chemically linked to the Afar plume occurred through the west margin of Arabia (Bosworth and Stockli, 2016). Regional Upper Oligocene to Lower Miocene magmatic activities were synchronous with the northward fast spread of the Red Sea/Gulf of Suez to the Mediterranean at 24 ± 2.2 Ma (Bojar et al., 2002; ArRajehi et al.,

2010). A corresponding rift shoulder uplift that was initiated is recorded in the AFT and AHe data and the thermal history modeling along the central and northern Red Sea (Kohn and Eyal, 1981; Omar et al., 1987; 1989; Szymanski et al., 2016; Morag et al., 2019; Mansour et al., 2021). An episode of erosional cooling during the Early Oligocene was documented in thermochronological data and burial history models of northern ANS (Avni et al., 2012; Feinstein et al., 2013; Naylor et al., 2013). Thermochronological data from the central ANS recorded Paleogene thermal stability (Szymanski et al., 2016), which recommended a localized nature of the Early Oligocene cooling event within northern Egypt and the Levant (Boone et al., 2021). Therefore, it was interpreted as being a reaction to a Late Eocene tectonic reorganization through the north of the Arabian and African margins which formed the Syrian Arc system (Bosworth and McClay, 2001; Boone et al., 2021).

The ANS is exposed around the Red Sea coastline of the African and Arabian plates (Figure 1). It is formed during the EAO (ca. 900–650 Ma) by a collision between the East and West Gondwana (McWilliams, 1981; Stern, 1994; Meert et al., 2011; Johnson, 2014). The Mozambique Ocean's juvenile crust was emplaced above arc-related rocks along numerous arc-arc and arc-continent suture zones, metasediments, and igneous intrusions of the Middle Cryogenian–Ediacaran (ca. 790–560 Ma), which accreted westerly into the Saharan Metacraton at ca. 650–580 Ma, marking the final consolidation stage of the ANS terrane (Johnson et al., 2011; Fritz et al., 2013; Johnson, 2014; Abd El-Wahed and Hamimi, 2021). Finally, post-tectonic granites were intruded no later than ca. 550 Ma (Fritz et al., 2013).

The ANS was eroded before the end of the Cambrian and buried beneath Phanerozoic sedimentary succession, starting with a series of fluvio-marine succession; it also started with Lower Cambrian fossils (Said, 1990; Seilacher, 1990; Bosworth et al., 2005). A period of tectonic stability post-dates the Cambrian as indicated by the deposition of platform sedimentation (Alsharhan and Nairn, 1997). That tectonic stability was occasionally interrupted by a series of uplifts recorded by un-conformities within the Lower Paleozoic sedimentary succession (Vermeesch et al., 2009). Then, the tectonic event of the Variscan or the Hercynian activated through Devonian–Carboniferous times via the impact of the Gondwana and the Laurasia that caused a southward tectonic reversal and a significant uplift and erosion of the Lower Paleozoic sediments by the Late Carboniferous time (Gvirtzman and Weissbrod, 1984; Klitzsch, 1986; Bojar et al., 2002; Stampfli et al., 2002; Craig et al., 2008; Dixon et al., 2010). The Eastern Mediterranean Sea was opened through the Triassic–Lower Jurassic (Garfunkel and Derin, 1985). Then, the Gondwana began breaking apart during the Jurassic–Cretaceous that caused localized volcanic flows and the restoration of northward tectonism in the northern ANS region (Hashad, 1978; Garfunkel and Derin, 1985; Klitzsch, 1986; Meneisy, 1986). The mid-Atlantic opening during the Middle Jurassic caused the African plate to move to the east with respect to Eurasia causing sinistral shearing, N-S and NW-SE normal faults, substantial magmatism with alkaline affinity, and development of the Syrian Arc folds system (Said, 1962; Dewey et al., 1973; Awad, 1984; Sestini, 1984; Girdler, 1985; Greiling et al., 1988). The rift system of the Red Sea/Suez rift initiated by the Oligo-Miocene caused exhumations and rock removals along their flanks, outcropping the ANS basements and forming basic dykes and systems of normal faults.

2.1 The ANS rock suits

The basement suits of the ANS in the NED mainly consisted of 1) metamorphic rocks belonging to the EAO island arc phase which stretched between 820 and 750 Ma (Kröner et al., 1994; Mansour et al., 2022a). This suite was represented in the area of study by metabasaltic andesite with a schistosity texture that was intruded by latterly developed granitic suites (El-Wakel et al., 2021). 2) The synorogenic suite which developed during a compressional setting that was dominant in the time span between ca. 750 and 610 Ma. (Stern and Hedge, 1985; Mansour et al., 2022a). It is represented in mainly the northern G. Umm Murakhat by dioritic and granodioritic rocks (Figure 2) that are frequently cut by chemically bimodal dykes. 3) The Late Precambrian Hammamat molasse sediments (ca. 590 Ma; Willis et al., 1988) that are intruded, in the area of study, by post-orogenic granitoids. This suite is restricted in the G. Loman region to the northern and northeastern parts of the area of study (Figure 2). 4) Post-orogenic suites of granitoids and dyke swarms that developed during the ANS extensional collapse stage between ca. 610 Ma and 550 Ma (Stern and Hedge, 1985; Platt and England, 1993; Mansour et al., 2022a; Mansour et al., 2023a). This suite is represented mainly in the area of study by monzogranitic and syenogranitic rocks that are traversed by dykes and quartz veins and are contaminated by sub-rounded xenoliths of the older suites (El-Wakel et al., 2021).

Structurally, El-Wakel et al. (2021) reported three phases of deformation in the studied area; two of them are compressional with maximum compressional axis trending N81°W and N13°W. The third phase of deformation was extensional with an N-S trending maximum tension force (Figure 2).

2.2 Sedimentological sequence

The integration of the sedimentological succession of NED which documents the depositional environments' major changes and rock exhumation periods (Figure 3) with our thermochronological data will enable documenting the correlation between the cooling and exhumation events.

The lithostratigraphic sequence in the Gulf of Suez and northern Red Sea region ranges from the Cambrian to present times (Figure 3) and can be classified into.

- A) The Palaeozoic succession (Figure 3), which was originally divided into three mappable units (Barron, 1907; Hassan, 1967; Said, 1971). A1) The Qebliat Group (Cambrian age, ~130 m thick) formed from cycles of fluvial to near-shore marine sediments (Hassan, 1967; Said, 1971; Bosworth et al., 2005). A2) The Um Bogma Formation (Carboniferous age, ~225 m thick) comprises dolomite, sandy marl, and intercalations of silt and sandstone (Kora, 1984; McClay et al., 1998). A3) The Abu Thora Formation (Carboniferous age, ~214 m thick) comprises varicolored interbedded fluvial sandstone with nearshore marine sandstone, siltstone, shale, and locally thin coal seams. The upper part of the Abu Thora Formation contains basalt sills at several localities (Weissbrod, 1969; Kora, 1984). By the end of the

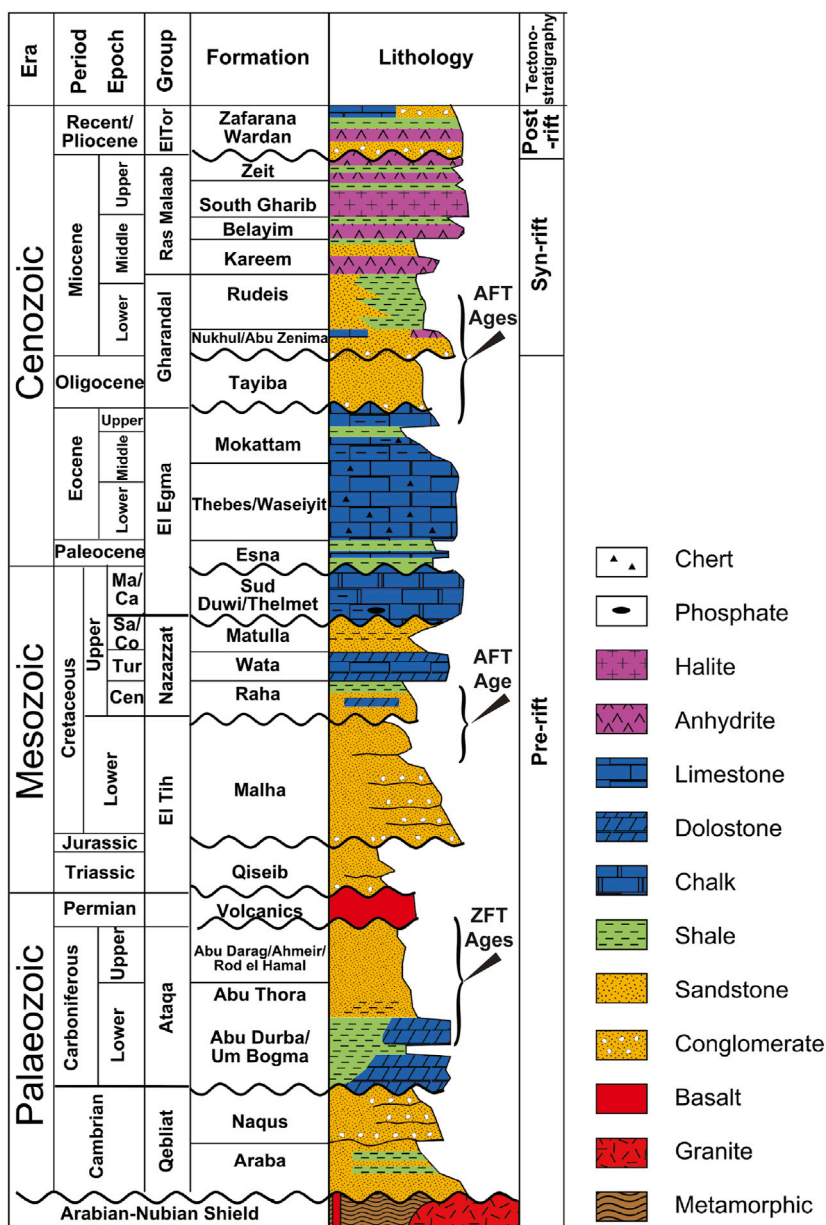


FIGURE 3 The simplified stratigraphic column of the northern Red Sea/Suez rift area (modified after Darwish and El Araby, 1994).

Carboniferous, the Gulf of Suez region was uplifted as indicated by a lack of any Permian marine sediments (Klitzsch and Wycisk, 1987; Klitzsch, 1990).

- B) The Mesozoic succession in the Gulf of Suez and the northern Red Sea region spans the Triassic to the Late Cretaceous (Figure 3). B1) The Qiseib Formation (Triassic age, ~327 m thick) consists of a lower variegated shale, siltstones, sandstones, and an upper thin clastic carbonate unit (Abdallah and El-Adindani, 1963; Weissbrod, 1969). B2) The Malha Formation (Lower Cretaceous age, ~149 m thick) comprises a lower Member of shale, clay, sandstone with conglomerate, and an upper Member of tabular and cross-bedded sandstone (Sultan, 1985; Abu-Zied, 2007; Kassem et al., 2020). B3) The Raha to

Sudr Formations (Upper Cretaceous age) represent a shallow marginal marine environment characterized by a mix of clastic and carbonate sequences (Osman, 1954; El Sharawy and Nabawy, 2016; Shehata et al., 2020; Shehata et al., 2023).

- C) The Cenozoic sequence spans the Palaeocene to Quaternary (Figure 3) and consists of C1) The Esna Formation (Palaeocene age, ~35 m thick). This consists of dark-greenish shale units and 1 m carbonate thin beds (Said, 1990). C2) The Thebes and Mokattam Formations (Lower Eocene and Middle-Upper Eocene age, respectively). This is represented mostly by chalky limestones with thin-bedded flint bands (Said, 1962; McClay et al., 1998; El-Azabi, 2006). C3) The Tayiba Formation (Oligocene age, ~152 m thick). This

unconformably overlies the Mokattam Formation (Ezz et al., 2016) and marks the transition from the pre-rifting Eocene marine sediments to the Early Miocene rift-forming transgression sediments (Refaat and Imam, 1999). C4) The Nukhul (Abu Zenima) Formation (Lower Miocene age, ~100 m thick). This unconformably overlies the Tayiba Formation and contains alluvial and volcanic deposits from the early syn-rift stage (Moustafa and Yousif, 1993; El-Anwar, 2019). C5) The Rudeis Formation (Lower-Middle Miocene age, ~191 m thick). This conformably overlies the Nukhul Formation and is characterized by deep marine sediments (El-Heiny and Martini, 1981; Sallam et al., 2019). C6) The Kareem, Belayim, South Gharib, and Zeit Formations (Middle-Late Miocene age, ~1,250 m thick). They conformably overlie the Rudeis Formation and each other. They are dominated by evaporites and intercalations of sandstones and shales (Tewfik et al., 1992; Darwish and El Araby, 1994; Sallam et al., 2019). C7) The Zafarana Warden Formation (Pliocene age, ~120 m thick). This is represented by sandstone and clay streaks (Tewfik et al., 1992; Sallam et al., 2019).

2.3 Research questions and published data

A debate concerning additional thermal print and plume effect during the northern Red Sed development still exists. The effects and magnitude of different regional tectonic events on the ANS involve the NED terrain (Steckler, 1985; Omar et al., 1989; Omar and Steckler, 1995; Feinstein et al., 1996; Bosworth et al., 2015; Mansour, 2016; Morag et al., 2019). Reconstructing the thermal-tectonic history of the rift flank is capable of providing new insights into these debates, especially with the obvious variation in the topographic growth across the RSRS (Figure 1B). The implication of different low-temperature multi-thermochronometer techniques has proven to be an effective thermal-tectonic history reconstruction tool in different geologic settings (Morag et al., 2019; Boone et al., 2021; Mansour et al., 2022b).

Previously conducted thermochronologic research on the northern segment of the ANS report a prolonged history of cooling with irregular exhumations through fault-bound blocks (Kohn and Eyal, 1981; Omar et al., 1987; 1989; Kohn et al., 1997; Vermeesch et al., 2009; Feinstein et al., 2013; Mansour, 2016; Mansour et al., 2021; Mansour et al., 2023b). The Suez rift flanks provided ZFT cooling age ranges between 674 ± 77 Ma and 381 ± 26 Ma (Mansour, 2016; Mansour et al., 2023b), AFT cooling age ranges between 485 ± 18 Ma and 11 ± 2 Ma (Kohn and Eyal, 1981; Omar et al., 1989; Kohn et al., 1997; Morag et al., 2019; Mansour et al., 2021; Mansour et al., 2023b), and dated AHe samples from 125 ± 5 Ma to 20 ± 2 Ma (Morag et al., 2019). The Aqaba rift flanks yielded AFT cooling age ranges from 266 ± 14 Ma and 11 ± 1 Ma (Kohn and Eyal, 1981; Feinstein et al., 2013). In the vicinity of the region of Eilat, the reported $^{40}\text{Ar}/^{39}\text{Ar}$ samples show ages of ca. 536 Ma (Vermeesch et al., 2009), ZFT age ranges from 372 ± 27 Ma to 292 ± 22 Ma (Kohn et al., 1992; Vermeesch et al., 2009), and dated AHe samples from 458 Ma to 205 Ma (Kohn et al., 2019). AFT detrital-dated samples vary between 329 ± 37 Ma and 258 ± 18 Ma and AHe cooling ages between 206 Ma and 12 Ma (Vermeesch et al., 2009; Kohn et al., 2019). The Western flank of the Red Sea at the

NED yielded SFT (FT in sphene) cooling age ranges from 411 to 338 Ma (Bojar et al., 2002), cooling ages of ZFT range from 367 to 314 Ma (Bojar et al., 2002), and cooling ages of AFT range between 190 ± 8 Ma and 29 ± 2 Ma (Omar et al., 1987).

3 Methods and techniques

The fission-track (FT) low-temperature thermometry technique is based on the radiation damage (etchable tracks) of the spontaneous ^{238}U fission accumulation in the crystal lattice (Wagner, 1972). The retention and annealing of these tracks of fission are sensitive to a temperature zone that vary with different minerals (Gleadow and Duddy, 1981; Yamada et al., 1995), which enables thermal-tectonic (t-T) history reconstruction.

We have collected 11 samples from the Gabal Loman area at the western flank of the Red Sea (Figure 2). The collected samples belong to the Precambrian rock suits evading any possible heating effect of later Phanerozoic intrusives. Only seven samples out of 11 provided adequate zircon grains and/or apatite grains to apply FT thermochronometry (Figure 2).

The Donelick et al. (2005) methods of minerals separation were used to extract zircon and apatite grains from the whole rock samples. Apatite-mounted grains were chemically etched in 5.5N HNO_3 at $20^\circ\text{C} \pm 1^\circ\text{C}$ for 20 s to reveal spontaneous tracks (Gleadow et al., 1983). Zircons mounts were etched in a NaOH — KOH eutectic melt at $220^\circ\text{C} \pm 5^\circ\text{C}$ (Garver, 2003) for 210–240 min. These conditions of chemical etching were applied to be compatible with the modeling code of Ketcham (2005). We have used the Laser Ablation Inductively Coupled Plasma Mass Spectrometry (LA-ICP-MS) at Kanazawa University, Japan, to measure concentrations of the U directly (Hasebe et al., 2004). In this study, the intensity of the Uranium signal was calibrated against silicate glass reference material SRM 610 produced by the National Institute of Standards and Technology (NIST 610) (Longerich et al., 1996), in which the ^{238}U concentration was 456 ppm (Carpenter and Reimer, 1974; Pearce et al., 1997). During data processing, the ^{43}Ca was considered as the interior normal to apatites according to the previously reported data (Barbarand et al., 2003). ^{29}Si was an internal standard tacking the chemical composition (Longerich et al., 1996; Pearce et al., 1997).

NIST SRM 612 was considered the secondary normal for the U-concentration measurements, and it yielded a concentration of $(37.5 \pm 0.9 \mu\text{g/g})$ in concordance with published data (Carpenter and Reimer, 1974; Walder et al., 1993; Pearce et al., 1997). The obtained ages and standard errors were produced by IsoplotR (Vermeesch, 2018).

For thermal history modeling, all the AFT data (single-grain cooling ages, c-axes-projected HCTs, and Dpar) were modeled using the multi-kinetic annealing model of Ketcham (2005). The initial Neoproterozoic age (at depth) was near the surface before the Cambrian (as the ANS was eroded by this time); ZFT ages (whenever dated), AFT ages, and the Suez rift opening age were used as t-T constraints. To approach the most likely cooling history (best-fit t-T path), the initial inverse modeling was based on the best forward model with an excellent fit to the inputted thermochronologic data. Wide t-T constrains boxes (initial cooling, the Cambrian surface, ZFT cooling ages, AFT cooling

TABLE 1 Detailed fission-track data, ages, and sample descriptions for the dated zircons.

S.-Code	Elev	Coordinates Decimal		Lithology	²³⁸ U [μg/g]	n	ρ _s	N _s	χ ² [%]	W.M. Age	1σ
		N	E							[Ma]	[Ma]
GUM-01	390	27.04386°	33.60154°	Syenogranite	392.8	17	72.1	4302	0.7	322.2	18.4
GUM-05	425	27.15974°	33.42487°	Syenogranite	274.5	23	49.0	4725	0.9	319.4	16.4

Samples and zircon fission-track data represented as W.M.; weighted mean ages with 1-sigma (σ) uncertainties, calculated with IsoplotR (Vermeesch, 2018). S.-Code; samples code, Elev.; the elevation above sea level of each sample in meters, U; concentration of ²³⁸U in μg/g, n; number of apatites where tracks were counted, ρ_s; spontaneous tracks densities (10⁶ tr/cm²), N_s; number of counted fission tracks, χ²; chi-square test values, MSWD; Mean Sum Weighted Deviates. Bold values indicates the most important data in these table.

TABLE 2 Sample descriptions and AFT ages.

S.-Code	Elev	Coordinates Decimal		Lithology	²³⁸ U [μg/g]	n	ρ _s	N _s	χ ² [%]	W.M. Age	1σ	Lc	1σ	Dpar	1σ
		N	E							[Ma]	(μm)	(μm)	(μm)	(μm)	
GUM-01	390	27.04386°	33.60154°	Syenogranite	4.7	22	0.1	46	1.0	36.3	5.4	13.4	1.3	1.6	0.2
GUM-03	406	27.13687°	33.57771°	Granodiorite	7.0	20	0.1	51	0.9	33.5	4.8	13.3	1.0	n/a	n/a
GUM-05	425	27.15974°	33.42487°	Syenogranite	5.6	20	0.1	45	1.0	33.2	5.1	12.6	1.2	n/a	n/a
GUM-08	665	27.06407°	33.44805°	Syenogranite	6.0	20	0.1	64	1.0	33.5	4.3	13.3	1.7	n/a	n/a
GUM-10	362	27.22560°	33.36201°	Monzogranite	25.8	21	1.5	508	0.9	114.6	5.9	12.5	1.5	1.6	0.1

Sample information and apatite fission-track data were given as weighted mean ages with 1-sigma (σ) uncertainties and calculated with IsoplotR (Vermeesch, 2018), Lc mean; mean track length after c-axis correction, Dpar; mean, etch pit diameter. More details are provided in Table 1. Bold values indicates the most important data in these table.

ages, and the north RSRS initiation time) were considered as controllers for the behavior of the t-T models. The models principally were run till we reached 100 good t-T models. In the modeling code HeFTy, every t-T model has a value refereeing to its goodness of fit (GOF) with the top-value for comparison between the model prediction and the input data.

Cooling, exhumation rates, and episodic rock uplift were inferred by extraction from t-T models, assuming ca. 20°C surface temperature, and 25°C/km and 50°C/km geothermal gradients (Morgan et al., 1985; Omar et al., 1987; Vermeesch et al., 2009). Here, “rock uplift” is used to interpret the vertical movement of rocks during a specific cooling/exhumation event, and “surface uplift” is equal to total rock uplift minus erosion (Lisker et al., 2009). In this sense, the rock uplift was calculated basically for each cooling event by multiplying the exhumation rate by the duration of that event.

4 Results

Two samples out of 11 produced dependable zircon grains for the ZFT technique (Table 1), and five samples produced accountable apatite grains for the AFT technique (Table 2). From AFT-analyzed mounts, two samples produced adequate horizontally confined tracks (HCTLs) for thermal history modeling. The produced FT

results are introduced in Table 1, Table 2, conferring to the recommendations of Hurford. (1990).

4.1 ZFT thermochronometer

The ZFT-analyzed mounts satisfy the Chi-square (χ²) test of age homogeneity (Table 1). The concentrations of uranium vary from ca. 393 to 275 μg/g (Table 1). The resulting weighted mean ZFT thermochronological ages and the related standard errors are 322 ± 18 Ma and 319 ± 16 Ma (Figure 2), representing a typical cooling/exhumation through/within the zone of partial annealing (PAZ) of ZFT (240°C–200 °C; Bernet et al., 2009) ca. 321 ± 17 Myrs ago (Table 1).

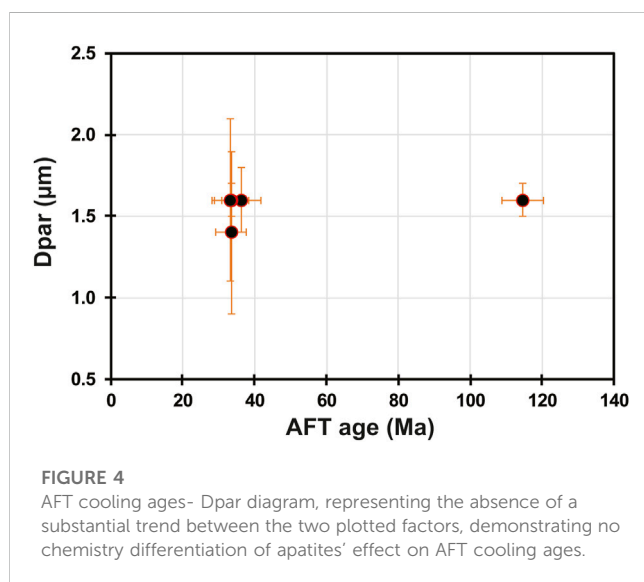
4.2 AFT thermochronometer

Obtained AFT cooling ages vary from 115 ± 6 Ma to 33 ± 5 Ma. The resulting cooling ages are detached spatially and temporally (Figure 2; Table 2); the oldest aged AFT sample GUM-10 has a Cretaceous age of 115 ± 6 Ma, indicating a typical cooling/exhumation through/within the PAZ of the AFT technique (110°C–60 °C; Gleadow et al., 1986; Donelick et al., 2005). The AFT age group with younger ages involves the closest

TABLE 3 The measured horizontal confined track length and Dpar data for the dated AFT samples.

Sample	HCTLs no.	HCTLs mean (μm)	HCTLs std. (μm)	HCTLs skew.	Lc mean (μm)	Lc std. (μm)	Lc skew.	Dpar no.	Dpar mean (μm)	Dpar std. (μm)	Dpar skew.
GUM-01	105	11.9	1.5	-0.411	13.4	1.3	-1.074	212	1.6	0.2	-0.262
GUM-03*	15	11.7	1.7	-0.371	13.3	1.0	0.005	26	1.6	0.1	0.912
GUM-05*	9	11.1	1.6	0.226	12.6	1.2	-0.390	20	1.6	0.5	0.120
GUM-08*	10	11.8	1.7	-0.184	13.3	1.7	-0.450	14	1.4	0.5	-3.073
GUM-10	101	11.0	1.9	-0.268	12.5	1.5	-0.746	215	1.6	0.1	-0.300

GUM-01; sample code, GUM-03*; samples with inadequate number measured HCTLs, HCTLs no.; measured horizontal confined tracks number, HCTLs mean; mean of the HCTLs, std; standard deviation, skew; skewness of distribution relative to the mean value, Lc mean; mean track length after c-axis correction, Dpar mean; mean, etch pit diameter. Bold values indicates the most important data in these table.



four samples closer to the Red Sea, which comprises Eocene-Oligocene ages between 36 ± 5 Ma and 33 ± 5 Ma (Figure 2), indicating a typical cooling/exhumation through/within the PAZ of the AFT technique at ca. 35 ± 5 Ma (Figure 2; Table 2).

The HCTLs that were corrected to the c-axis (Lc) yielded length ranges from 13.4 ± 1.3 μm to 12.5 ± 1.5 μm (Table 3). We measured 487 Dpars as a total, producing value ranges between 1.6 ± 0.5 μm and 1.4 ± 0.5 μm (Table 3). A systematic relationship between the apatite FT ages and the Dpar values is absent (Figure 4).

4.3 Time-temperature history modeling

The thermal history of the area of study was reassembled using the computer software modeling HeFTy v1.8.3 (Ketcham, 2009; Ketcham et al., 2009). The used Monte Carlo algorithm required t-T constraints that were defined by the user. The introduced constraint boxes were constructed according to the resulting ZFT and AFT cooling ages and geological events whose ages are well-known; these

events are the post-accumulation event of erosion (PAEE) that was responsible for the removal of the whole ANS by the Cambrian time and the Red Sea initiation during the Oligo-Miocene time (Figure 5). The constraint extensions on both the X and Y-axis were constructed according to the uncertainty in the timing of every one of them. Other constraints (age-based) were constructed according to the obtained cooling ages; else, they were widely constrained, providing more liberty for the t-T paths. The accuracy of the produced t-T paths mainly counts on the number of the used HCTLs. Thus, we have only modeled samples with adequate HCTLs (Table 3).

The produced thermal history paths suggest two possible cooling/exhumation histories for the region of study: 1) the first is sample GUM-10 (Figure 5): affected by a Precambrian fast-cooling event which caused the sample to exhume to near the Earth's surface. Shortly after, the sample was affected by a slow reheating event that prolonged to the Devonian when another fast-cooling event initiated and exhumed the rock column to the AFT PAZ upper portion. Afterward, the rock column experienced a period characterized by slow cooling till the Eocene when a third cooling event caused it to be uplifted to its recent elevation (Figure 5). 2) The second is sample GUM-01 (Figure 5): affected by a Precambrian fast-cooling event to uplift the rock column to near the Earth's surface. Then, the rock column was affected by a slow reheating event that might have prolonged till the Cretaceous time when the sample experienced another fast-cooling event during the Jurassic-Cretaceous time, causing its exhumation to reach AFT PAZ. Afterward, the rock column was affected by a third cooling event during the Eocene to be uplifted to the recent altitudes (Figure 5). However, the sample GUM-01 model shows a wide range of cooling/exhumation possibilities extending from the Devonian to the Cretaceous.

From the modeled samples (Figure 5) and the obtained pre-ripped AFT cooling ages, no synchronous thermal anomaly to the northern Red Sea rifting (Oligocene-Miocene) was recorded on the t-T models; alternatively, the area of study was exhumed from ca. 60°C equivalent depths (Figure 5).

5 Discussion

The Gabal Loman area is exposed at the northern Red Sea's western flank, and its basement rocks enclose the whole regional geologic history

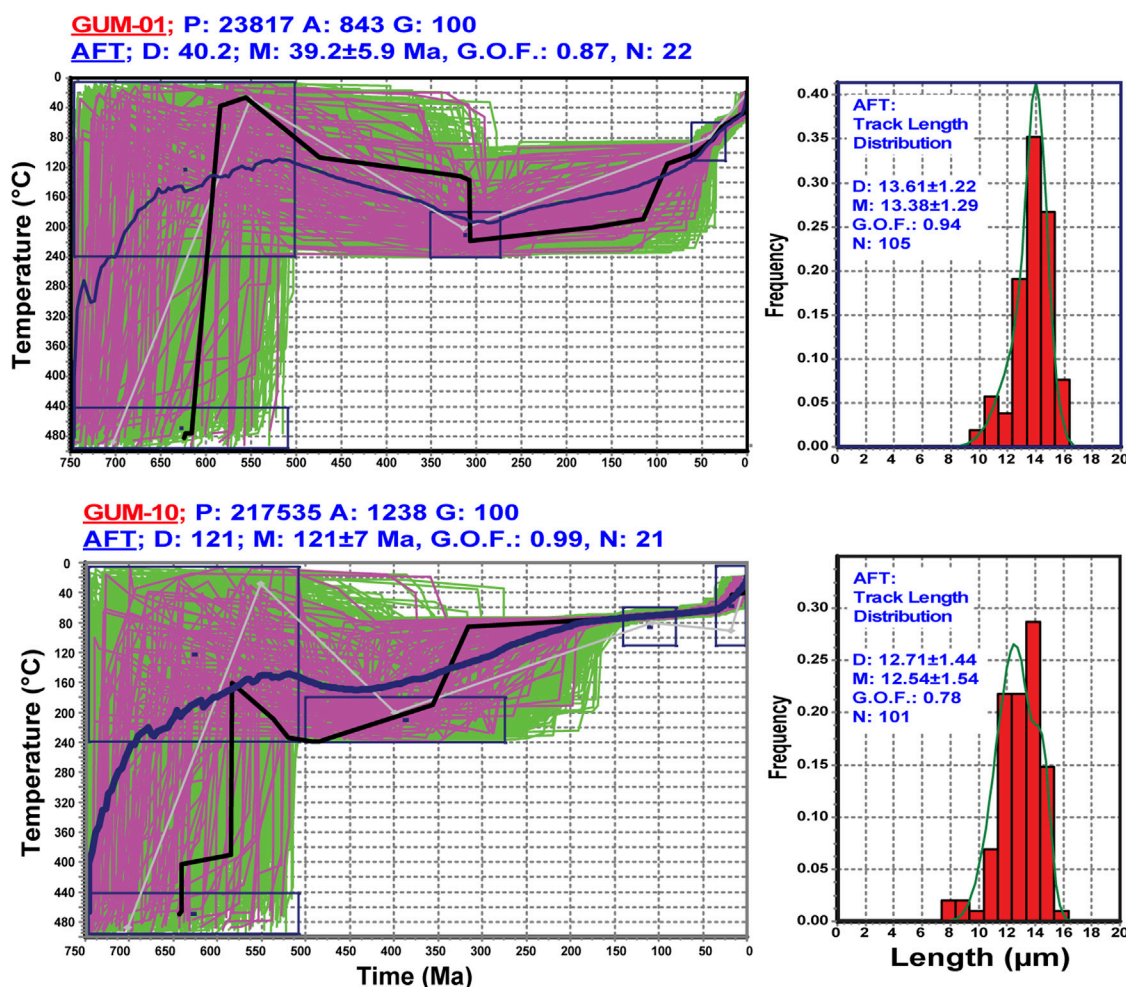


FIGURE 5

Thermal history models for samples obtained using HeFTy (Ketchum, 2005). The resulting t–T paths represent four levels of reliability: acceptable fit (green), good fit (purple), best fit (black), and weighted mean (blue) paths. Five constraints were used to limit the modeling randomness, where the 1st represents the initial box at depth, the 2nd represents the post-accretion-related exhumation event, the 3rd shows the ZFT age, the 4th shows the AFT age, and the 5th represents the Suez Rift opening. Where, SRR-01: sample code, P: number of inverse iterations, A: acceptable fit models' number, G: good fit models' number, D: calculated AFT ages and CLs (1- σ error), M: model calculated AFT ages and CLs, G.O.F. goodness of fit, N: number of single grains and CLs.

since its construction during the Neoproterozoic till the development of the northern Red Sea rift during the Oligo-Miocene time. Therefore, the tectonic history of the region is suitable for reconstructing and testing the different proposed models for Tertiary rift development.

The area of the study reactivated in reaction to the Hercynian tectonic events and the disintegration of Gondwana through the differential uplifts across fault-bounded blocks as indicated by differentiated AFT age groups, the time-temperature modeling, and the previously reported thermochronologic ages (e.g., Kohn and Eyal, 1981; Omar et al., 1987; 1989; Kohn et al., 1997; Vermeesch et al., 2009; Feinstein et al., 2013; Mansour, 2016; Mansour et al., 2021). Therefore, further detailed structural analyses considering this selective uplifting nature may disclose these faults' kinematic characteristics.

The low-temperature thermochronology thermal sensitivity would enable the basin burial/exposure history (e.g., Zheng et al., 2003; Li et al., 2017). The AFT temperature sensitivity zone is

identical to the hydrocarbon maturation temperature zone, which could enable basin evaluation from a hydrocarbon reservoir exploration perspective (Gleadow et al., 1983). One of the main objectives of this study is to provide a tectonic-thermal model for the RSRS formation and development through time as an example of the evolution of rifts with similar geologic settings. However, further basins-sampled studies could detect the tectonic-related stratigraphic variation within the basin and the rift-related structural variations which will lead to a better basin and reservoir evaluation.

5.1 ZFT thermochronometry

The analyzed mounts have passed Chi-square (χ^2) homogeneity test, indicating the absence of any evidence of multiple age populations (Table 1).

The yielded ages (average 321 ± 17 Ma; Figure 2) are concordant with published ZHe and ZFT thermochronological ages from different localities of the ANS. These reported Carboniferous thermochronological ages have introduced activated uplifts in response to the Devonian-Carboniferous tectonic activities (Kohn et al., 1992; Bojar et al., 2002; Vermeesch et al., 2009; Mansour, 2016). This regional uplift is concordant with changes in the regime of the deposition from the Um Bogma Formation (the Lower Carboniferous, marine affinity) to the Abu Thora Formation (the Upper Carboniferous, erosional nonmarine affinity) (Figure 3).

5.2 AFT thermochronometry

The obtained AFT cooling ages range from ca. 115 ± 6 Ma to ca. 33 ± 5 Ma. These ages are separated into two geographically differentiated regions, demonstrating a differential response to the different thermal-tectonic events (Figure 2). The geographic differentiation is constant with differential uplifts that were controlled by block movements through boundary faults that characterize the ANS different regions (Kohn and Eyal, 1981; Omar et al., 1987; Omar et al., 1989; Kohn et al., 1997; Vermeesch et al., 2009; Mansour, 2016). Furthermore, the AFT cooling age of the older mount (Cretaceous; GUM-10) is consistent with the stratigraphic sequence showing a change in the deposition environment from the formation of Wata (marine affinity) to the formation of Matulla (nonmarine affinity) (Figure 3), which suggests synchronized exhumations. In contrast, AFT younger-aged groups (Eocene-Oligocene; GUM-01, GUM-03, GUM-05, and GUM-08) are concurrent with previously reported AFT ages in the northern segment of the ANS (Omar et al., 1989; Morag et al., 2019) and the Eocene-Oligocene unconformity and changes in the deposition environment from the Mokattam Formation (marine affinity) to the Tayiba Formation (nonmarine clastics) (Figure 3).

The obtained cooling ages were considered a little older than the producing equivalent rock uplifting activities; this is indicated by a prolonged resident time in AFT PAZ (Figure 4). This conclusion was additionally maintained through the younger-aged AFT sample has 33 ± 5 Ma age, which predates the Red Sea initiation. Consequently, the region has not experienced any higher temperatures than the AFT closure temperature (110°C) since the Eocene-Oligocene boundary. Furthermore, uplifting from AFT PAZ is supported by thermal history modeling and histograms of the track lengths distribution as the majority of the Lc distributions yield a negative skewness (Figure 4).

5.3 Thermal history modeling

The t-T modeling represents different rapid cooling events; these could be represented as rock uplifts if associated with the obtained cooling ages, the well-known geologic events, and the sedimentological succession. These cooling/uplifting events are 1) The Precambrian uplifting event (Figure 4). This is initiated in response to the PAEE and sedimentation of the fluvio-marine Cambrian deposits. 2) Devonian-Carboniferous time uplifting/cooling activity (Figure 4). This is emphasized by our ZFT ages. During this event, the terrain uplifting in the RSRS region was a

reaction to the tectonic activity of the Hercynian that caused a change in the sedimentological nature from the Early Carboniferous time Um Bogma marine sediments to the Late Carboniferous time Abu Thora erosional sediments (Figure 3). This uplift caused rock erosion of more than 2.5 km of an Early Palaeozoic succession plus part of the underlying ANS rocks (Kohn et al., 1992; Moustafa and Yousif, 1993). 3) The Cretaceous uplifting activity (Figure 4). This happened when the studied region responded to the Gondwana breakup by differential exhumations. This event caused localized uplifts in northern Africa and the northern Red Sea region (Shalaby and Shawky, 2014; Shalaby, 2017). Additionally, it produced conglomeratic sandstone erosional deposits dominance and multiple hiatus throughout the whole Cretaceous (Figure 3). The effect of this event is previously reported as tectonically-caused structure (strike-slip faults) and major cooling events (Bojar et al., 2002; Feinstein et al., 2013). This regional differential exhumation nature of the ANS is a reaction to the tectonic activities of the Hercynian and the disintegration of the Gondwana which is widely reported in earlier thermochronologic studies (Kohn and Eyal, 1981; Omar et al., 1987; Omar et al., 1989; Kohn et al., 1992; Vermeesch et al., 2009; Feinstein et al., 2013; Mansour et al., 2023b). This differential uplifting nature was probably governed by the activation of faults according to the different directions of the stress field for each of them. 4) Oligo-Miocene uplifting event (Figure 4). This is seemingly concordant with the Red Sea rifting (e.g., Bosworth and Taviani, 1996; Bosworth and Mc Clay, 2001). The produced thermal history modeling (Figure 4) and older rifting AFT cooling ages (Table 2) indicate the absence of any thermal overprint synchronous to the northern Red Sea opening, and the rift shoulders uplifted only from depths comparable to ca. 60°C (Figure 4).

5.4 Cooling and rocks exhumation

The exhumation of buried rocks in rift basins is independent of their cooling events, which are determined by thermochronological data; however, it can be predicted if these cooling events are coupled with the reported geologic events and stratigraphic sequence. The exhumation amount that accompanied each of the reported tectonic events could be calculated from the obtained thermochronologic ages and the corresponding PAZ. The paleo-geothermal gradient is not known; therefore, we used a variety of possible geothermal gradients from the recent ($25^\circ\text{C}/\text{km}$) to the expected during active tectonism ($50^\circ\text{C}/\text{km}$). Afterward, the resulting rates were correlated to the stratigraphic sequence and compared to the synchronic tectonic events. This approach supports obtained cooling ages/events representative for major rock uplifting events: 1) PAEE event. It caused erosion of the entire ANS to transform it into a peneplain surface (Kolodner et al., 2006); consequently, the recent rock exposures isostatically exhumed from their depths of emplacement to near the Earth's surface. 2) The Hercynian (Variscan) tectonic activity. This influenced the Egyptian ANS partially through differential exhumations and resulted in the complete removal of the Early Palaeozoic succession and a portion of the basement rocks (Stampfli et al., 2002). This event affected the studied region by rock uplift from depths equivalent to the ZFT PAZ temperatures (240°C – 200°C) to ca. 60°C equivalent depth. This amount of exhumation corresponds to ca. 4 km 3) The

Gondwana disintegration activity. This produced convergence between the African and the Eurasian plates, which caused a total rock exhumation of ca. 2.4 km in NED and Sinai (Moustafa and Fouda, 2014). This local influence on the studied region is indicated by the modeling of the t-T history (Figure 5). It is suggested that the effect of the Gondwana breakup event is combined with the Hercynian event to uplift the ANS in the area of study from depths equivalent to ZFT PAZ (240°C–200 °C) to depths equivalent to ca. 60 °C. (4)The northern Red Sea opening. This resulted in rift shoulders exhumation at Wadi Miar with ca. 2.4 km, southern Sinai (Morag et al., 2019). However, in the current area of study, the northern Red Sea development resulted in a rock uplift of ca. 1.2 ± 0.4 km.

5.5 Implications to the Suez Rift

The Gulf of Suez is recognized as a non-volcanic rift except for localized simultaneous basaltic subsurface eruptions and surface dikes despite southern Sinai having an anomalously 2.5 km elevated rift flank. Recently, normal faults associated with 23 Ma subsurface basaltic flood of a relatively constant thickness are being reported in the Cairo-Suez region (Bosworth et al., 2015). They are compositionally similar to the Afar flood basalt in the East African Rift which shows a similar magmatic source to the rifting processes and the absence of pre-rift high topography. The pre-rift low topography is documented by the modest erosional-constituting sedimentary formations (300–500 m) in the rift valley (Garfunkel, 1988) and supports no plume-caused doming which would have produced elevated topography and enflamed amounts of erosional preservations. Additionally, Bosworth et al. (2015) delivered 3D seismic interpretations for circular depressions in the Suez rift grabens which were formed through magma evacuation from below. While a syn-rift deep-seated thermal anomaly would last for more than 60 Myr (Ebinger and Sleep, 1998; Bosworth et al., 2015), this is not the case here, suggesting a more localized and limited source of magmatism. Melts lateral migration from the preexisting Afar plume could provide a more localized source (Ebinger and Sleep, 1998; Bosworth et al., 2015). From southern Sinai, Steckler. (1995) suggested lateral heat transfer from Sinai Triple Junction as a source for the exceptional elevations, while Morag et al. (2019) reported concurrent exhumation, rift initiation, and magmatism, which was interpreted as an indicator of mantle plume involvement. Additionally, the Afar plume northward extension toward the margin of the Arabian plate has been reported (Hansen et al., 2012).

The obtained thermochronologic data yields no AFT age resetting, and the distribution of HCTLs supports uplift from the AFT PAZ (110°C–60 °C), while the t-T models restrict this temperature to ca. 60 °C (Figure 5). The recent geothermal gradient is 25 °C (Morgan et al., 1985; Feinstein et al., 1996), and its doubling is expected during the rifting active period (Omar et al., 1989; Kohn et al., 1992), which suggests rift flank uplift at the studied area from depths of ca. 1.2 ± 0.4 km. These elevations are consistent with the current RSRS western flank low topography (Figure 1B), with the highest peak of ca. 1,018 m at Gabal Loman. Considering the facts that the RSRS and Afar basaltic eruptions are compositionally similar, the Suez rift flanks uplifted only through

its southern half (Figure 1A); the anomalously high flank is restricted to the southern part of the eastern flank at southern Sinai (Figure 1B), reducing the eastern rift flank uplift from the south (2.4 km; Morag et al., 2019) to the north (1.2 ± 0.4 km; Mansour, 2016) (Figure 1B; cross sections AA' and BB'); the western flank low topography accompanied the exhumation (1.2 ± 0.4 km; this study) and the vast amount of the Cenozoic volcanism on the Arabian Shield. We proposed a mechanical rift type for the RSRS additional east-southward thermal overprint caused by lateral migration of melts from the Arabian marginal plume as a source for the exceptional southward elevations of the eastern rift flank and the synchronous basaltic eruptions.

The age of the basaltic volcanism associated with the Suez Rift initiation (23 Ma) overlaps with the ages of the rift-related dikes in the Egyptian Eastern Desert, the Sinai, and western Arabia (Bosworth and Stockli, 2016; Nuriel et al., 2017). This suggests a single and rapid rifting pulse as the Red Sea spread northward through the Suez rift until the Dead Sea Transform (DST) fault activated and migrated the stress field. The DST activation (20–18 Ma; Nuriel et al., 2017) caused the Suez rift flanks exhumation deceleration (25–18 Ma; Morag et al., 2019), while it continued along the Red Sea flanks (15 Ma; Szymanski et al., 2016).

6 Interpretation

The ZFT ages are represented by Carboniferous ages of ca. 321 ± 17 Ma, indicating a synchronous rapid exhumation passing through the ZFT closure temperature at this time, while the AFT cooling ages are ranging over two age spans of Cretaceous of 115 ± 6 Ma and Eocene-Oligocene of ca. 35 ± 5 Ma. These two different clusters of thermochronologic ages suggest two different thermal-tectonic histories that are not the formation age of lithology-related ages, rather it indicates differentiation in the uplift-erosion history.

The resulting cooling ages and the thermal history modeling yielded four uplifting/cooling tectonically-induced activities: 1) Precambrian PAEE. This was induced by the EAO producing continental thickening and plutonism through the Neoproterozoic time which influenced the entire ANS by erosion, rock removal, and, consequently, exhumations of the studied area closer to the Earth's surface through isostatic rebound as indicated by our time-temperature modeling (Figure 5). Then, the ANS was squeezed under an Early Palaeozoic succession to depths of ca. 2.5 km. 2) The Devonian- Carboniferous Hercynian tectonic activity. This produced rock exhumations (ca. 4.2 ± 1.4 km) and sample cooling from PAZ temperatures of ZFT to temperatures of ca. 60 °C. The Hercynian tectonic event is responsible for the erosion of the Lower Palaeozoic sequence and portions of the ANS basement rocks. This event is supported by the time-temperature modeling and the yielded ZFT ages (Figure 2; Figure 5). 3) Gondwana disintegration during the Cretaceous time. This produced exhumations with a localized nature as indicated by our time-temperature modeling (Figure 5). 4) Oligo-Miocene northern Red Sea initiation. This was accompanied by regional cooling and uplifts to the current elevations from ca. 60 °C equivalent depths. This rock exhumation is equal to ca. 1.2 ± 0.4 km. This event is supported by our time-temperature modeling and the resulting AFT ages (Figure 2; Figure 5).

The obtained AFT cooling ages predate the Oligocene-Miocene northern Red Sea/Suez rift initiation, and the Lc histograms indicate samples uplift from the AFT PAZ. The thermal history modeling indicates a rift-associated rock uplift from depths equivalent to ca. 60 °C (Figure 5) that corresponds to a rock exhumation of ca. 1.2 ± 0.4 km. These results document the absence of any thermal print on the studied region of the northern Red Sea rift's western flank.

7 Conclusion

The Gabal Loman area was developed during the EAO as part of the northern ANS. Then, the ANS was completely removed before the Cambrian time, and, consequently, a massive rock uplift took place to bring the currently exposed rocks near the Earth's surface. Afterward, an Early Palaeozoic sequence of ca. 2.5 km was deposited to bury the entire region beneath it. Afterward, the Hercynian tectonic activity was activated during the Devonian-Carboniferous time to exhume a rock column of ca. 4.2 ± 1.4 km. Then, the Gondwana disintegration was initiated during the Cretaceous time and might have caused differential exhumations in the studied region. The northern Red Sea/Suez rift system that was initiated during the Oligo-Miocene time caused rift shoulder exhumations of ca. 1.2 ± 0.4 km. Lastly, the rift shoulders were reshaped by nontectonic erosion to the recent altitudes.

The northern Red Sea/Suez rift system was initiated as a passive rift where the mechanical components are dominant and there was no additional thermal overprint, especially for the western rift flank.

Data availability statement

The datasets presented in this study can be found in online repositories. The names of the repository/repositories and accession number(s) can be found in the Mansour, Sherif (2023), "Gabal Oman", Mendeley Data, V2, doi: [10.17632/csg67znstr.2](https://doi.org/10.17632/csg67znstr.2).

References

- Abd El-Wahed, M., and Hamimi, Z. (2021). "The Egyptian nubian shield within the frame of the arabian-nubian shield," in *The Geology of the Egyptian nubian Shield, regional Geology reviews*. Editors Z. Hamimi, S. Arai, A. R. Fowler, and M. Z. El-Bialy (Switzerland: Springer), 15–51.
- Abdallah, A. M., and El-Adindani, A. (1963). Stratigraphy of upper paleozoic rocks of western side of Gulf of Suez PDF | PDF. *Geol. Surv. Egypt* 25, 1–18.
- Abu-Zied, R. (2007). Palaeoenvironmental significance of early cretaceous foraminifera from northern Sinai, Egypt. *Cretac. Res. Cretac. RES* 28, 765–784. doi:10.1016/j.cretres.2006.11.002
- Ahmed, A., Tiberi, C., Leroy, S., Stuart, G. W., Keir, D., Sholan, J., et al. (2013). Crustal structure of the rifted volcanic margins and uplifted plateau of Western Yemen from receiver function analysis. *Geophys. J. Int.* 193, 1673–1690. doi:10.1093/gji/ggt072
- Almalki, K., Betts, P., and Ailleres, L. (2015). The Red Sea – 50 years of geological and geophysical research. *Earth-Science Rev.* 147, 109–140. doi:10.1016/j.earscirev.2015.05.002
- Alsharhan, A. S., and Nairn, A. E. M. (1997). *Sedimentary basins and petroleum Geology of the Middle East*. Amsterdam, Netherlands: Elsevier. doi:10.1016/B978-0-444-82465-3.X5000-1
- ArRajehi, A., McClusky, S., Reilinger, R., Daoud, M., Alchalbi, A., Ergintav, S., et al. (2010). Geodetic constraints on present-day motion of the Arabian plate: Implications for Red Sea and Gulf of aden rifting. *Tectonics* 29, 482. doi:10.1029/2009TC002482
- Avni, Y., Segev, A., and Ginat, H. (2012). Oligocene regional denudation of the northern Afar dome: Pre- and syn-breakup stages of the Afro-Arabian plate. *Geol. Soc. Am. Bull.* 124, 1871–1897. doi:10.1130/B30634.1
- Awad, G. M. (1984). Habitat of oil in Abu gharadiq and faiyum basins, western Desert, Egypt. *AAPG Bull.* 68, 564–573.
- Balestrieri, M. L., Abbate, E., Bigazzi, G., and El Bedri Ali, O. (2009). Thermochronological data from Sudan in the frame of the denudational history of the nubian Red Sea margin. *Earth Surf. Process. Landforms* 34, 1279–1290. doi:10.1002/esp.1820
- Barbarand, J., Carter, A., Wood, I., and Hurford, T. (2003). Compositional and structural control of fission-track annealing in apatite. *Chem. Geol.* 198, 107–137. doi:10.1016/S0009-2541(02)00424-2
- Barron, T. (1907). *The topography and Geology of the peninsula of Sinai (western portion)*. Cairo: The Egyptian Geological Survey, 123–130.
- Batt, G. E., and Brandon, M. T. (2002). Lateral thinking: 2-D interpretation of thermochronology in convergent orogenic settings. *Tectonophysics* 349, 185–201. doi:10.1016/S0040-1951(02)00053-7
- Be'eri-Shlevin, Y., Eyal, M., Eyal, Y., Whitehouse, M. J., and Litvinovsky, B. (2012). The sa'al volcano-sedimentary complex (Sinai, Egypt): A latest mesoproterozoic volcanic arc in the northern arabian nubian shield. *Geology* 40, 403–406. doi:10.1130/G32788.1
- Bellahsen, N., Faccenna, C., Funicello, F., Daniel, J. M., and Jolivet, L. (2003). Why did Arabia separate from Africa? Insights from 3-D laboratory experiments. *Earth Planet. Sci. Lett.* 216, 365–381. doi:10.1016/S0012-821X(03)00516-8
- Bernet, M., Brandon, M., Garver, J., Balestrieri, M. L., Ventura, B., and Zattin, M. (2009). Exhuming the alps through time: Clues from detrital zircon fission-track thermochronology. *Basin Res.* 21, 781–798. doi:10.1111/j.1365-2117.2009.00400.x

Author contributions

All authors listed have made a substantial, direct, and intellectual contribution to the work and approved it for publication.

Funding

This research was supported by the Researchers Supporting Project number (RSP 2023R351), King Saud University, Riyadh, Saudi Arabia.

Acknowledgments

We thank Mohamed El-Bialy, Port Said University, for his helpful discussions with the first author.

Conflict of interest

The authors declare that the research was conducted in the absence of any commercial or financial relationships that could be construed as a potential conflict of interest.

The handling editor MAS declared a past co-authorship with the author SM.

Publisher's note

All claims expressed in this article are solely those of the authors and do not necessarily represent those of their affiliated organizations, or those of the publisher, the editors and the reviewers. Any product that may be evaluated in this article, or claim that may be made by its manufacturer, is not guaranteed or endorsed by the publisher.

- Bohannon, R. G., Naeser, C. W., Schmidt, D. L., and Zimmermann, R. A. (1989). The timing of uplift, volcanism, and rifting peripheral to the Red Sea: A case for passive rifting? *J. Geophys. Res.* 94, 1683. doi:10.1029/JB094iB02p01683
- Bojar, A. V., Fritz, H., Kargl, S., and Unzog, W. (2002). Phanerozoic tectonothermal history of the arabian-nubian shield in the Eastern Desert of Egypt: Evidence from fission track and paleostress data. *J. Afr. Earth Sci.* 34, 191–202. doi:10.1016/S0899-5362(02)00018-0
- Boone, S. C., Balestrieri, M. L., and Kohn, B. (2021). Thermo-tectonic imaging of the Gulf of aden-red Sea rift systems and afro-arabian hinterland. *Earth-Science Rev.* 222, 103824. doi:10.1016/j.earscirev.2021.103824
- Bosworth, W., Huchon, P., and McClay, K. (2005). The Red Sea and Gulf of aden basins. *J. Afr. Earth Sci.* 43, 334–378. doi:10.1016/j.jafrearsci.2005.07.020
- Bosworth, W., and McClay, K. (2001). *Structural and stratigraphic evolution of the neogene Gulf of Suez*. Egypt: a synthesis.
- Bosworth, W., and Stockli, D. F. (2016). Early magmatism in the greater red Sea rift: Timing and significance. *Can. J. Earth Sci.* 53, 1158–1176. doi:10.1139/cjes-2016-0019
- Bosworth, W., Stockli, D. F., and Helgeson, D. E. (2015). Integrated outcrop, 3D seismic, and geochronologic interpretation of Red Sea dike-related deformation in the Western Desert, Egypt – the role of the 23Ma Cairo mini-plume. *J. Afr. Earth Sci.* 109, 107–119. doi:10.1016/j.jafrearsci.2015.05.005
- Bosworth, W., and Taviani, M. (1996). Late quaternary reorientation of stress field and extension direction in the southern Gulf of Suez, Egypt: Evidence from uplifted coral terraces, mesoscopic fault arrays, and borehole breakouts. *Tectonics* 15, 791–802. doi:10.1029/95tc03851
- Burke, K., and Dewey, J. F. (1973). Plume-generated triple junctions: Key indicators in applying plate tectonics to old rocks. *J. Geol.* 81, 406–433. doi:10.1086/627882
- Burke, K. (1996). The African plate. *South Afr. J. Geol.* 99, 341–409.
- Carpenter, B. S., and Reimer, G. M. (1974). *Standard reference materials: Calibrated glass standards for fission track use*. Washington, DC: U.S. Department of Commerce.
- Cole, G., Al-Hajji, A., Colling, E., Halpern, H., Carrigan, W., Savage, G., et al. (1995). Petroleum geochemistry of the midyan and jaizan basins of the Red Sea, Saudi Arabia. *Mar. Petroleum Geol.* 12, 597–614. doi:10.1016/0264-8172(95)98087-1
- Corbeau, J., Rolandone, F., Leroy, S., Al-Lazki, A., Stork, A. L., Keir, D., et al. (2014). Uppermost mantle velocity from pn tomography in the Gulf of aden. *Geosphere* 10, 958–968. doi:10.1130/GES01052.1
- Craig, J., Luening, S., and Beswetherick, S. (2008). Structural styles and prospectivity in the precambrian and palaeozoic hydrocarbon systems of north Africa, in geology of East Libya. *Earth Sci. Soc. Libya, Tripoli* 163, 51–122.
- Darwish, M., and El Araby, A. (1994). Petrography and diagenetic aspects of some siliclastic hydrocarbon reservoirs in relation to rifting of the Gulf of Suez, Egypt. Geodynamics and sedimentation of the Red Sea—Gulf of aden rift system. *Egypt. J. Geol.* 3, 1–25.
- Dewey, J. F., Pitman, W. C., Ryan, W. B. F., and Bonnin, J. (1973). Plate tectonics and the evolution of the alpine system. *Geol. Soc. Am. Bull.* 84, 3137. doi:10.1130/0016-7606(1973)84<3137:PTATEO>2.0.CO;2
- Dixon, R. J., Moore, J. K. S., Bourne, M., Dunn, E., Haig, D. B., Hossack, J., et al. (2010). Integrated petroleum systems and play fairway analysis in a complex Palaeozoic basin: Ghadames-Illizi Basin, North Africa. *Geol. Soc. Lond. Pet. Geol. Conf. Ser.* 7, 735–760. doi:10.1144/0070735
- Donelick, R. A., O’Sullivan, P. B., and Ketcham, R. A. (2005). “3. Apatite fission-track analysis.” in *Low-temperature thermochronology*. Editors P. W. Reiners and T. A. Ehlers (Berlin, Boston: De Gruyter), 49–94. doi:10.1515/9781501509575-005
- Ebinger, C. J., and Sleep, N. H. (1998). Cenozoic magmatism throughout east Africa resulting from impact of a single plume. *Nature* 395, 788–791. doi:10.1038/27417
- EGPC (Egyptian General Petroleum Corporation) (1996). Oligocene and Miocene stratigraphy of the Gulf of Suez region. Report, Stratigraphic Committee, 142.
- El Sharawy, M. S., and Nabawy, B. S. (2016). Geological and petrophysical characterization of the lower senonian Matulla formation in southern and central Gulf of Suez, Egypt. *Arab. J. Sci. Eng.* 41, 281–300. doi:10.1007/s13369-015-1806-7
- El-Anwar, E. (2019). Geochemical studies of carbonates of the Tayiba Formation (upper Eocene), Abu Zenima area, west central Sinai. *Bull. Natl. Res. Centre* 43, 209. doi:10.1186/s42269-019-0240-5
- El-Azabi, M. H. (2006). “Sedimentological characteristics, palaeoenvironments and cyclostratigraphy of the middle Eocene sequences in Gabal el-Ramliya, Maadi-Sukhna stretch, north eastern Desert,” in *Egyptian 8th international conference on the Geology of arab world* (Cairo, Egypt: Springer).
- El-Bialy, M. Z. (2020). “Precambrian basement complex of Egypt,” in *The Geology of Egypt regional Geology reviews*. Editors Z. Hamimi, A. El-Barkooky, J. Martinez Frias, H. Fritz, and Y. Abd El-Rahman (Cham: Springer International Publishing), 37–79. doi:10.1007/978-3-030-15265-9_2
- El-Heiny, I., and Martini, E. (1981). Miocene foraminiferal and calcareous nannoplankton assemblages from the Gulf of Suez Region and correlations. *G. Col. Midderr.* 8, 101–108. doi:10.3406/geolm.1981.1159
- El-Wakel, E. S., El-Sundoly, H. I., El-Sayed, M. M., and Shalaby, M. H. (2021). Structural analyses and geological studies of the late precambrian basement complex in Wadi faliq el sahl–faliq el waar area, North Eastern Desert, Egypt. *Arabian J. Geosciences* 14, 2025. doi:10.1007/s12517-021-08399-z
- Ezz, A., Elhariri, T., and El, A. (2016). Mineralogical and geochemical studies of Eocene carbonate rocks at Wadi Tayiba and Wadi feiran areas, southwestern Sinai, Egypt. *Int. J. Sci. Eng. Appl. Sci. (IJSEAS)* 2, 2395–3470.
- Feinstein, S., Eyal, M., Kohn, B. P., Steckler, M. S., Ibrahim, K. M., Moh’d, B. K., et al. (2013). Uplift and denudation history of the eastern Dead Sea rift flank, SW Jordan: Evidence from apatite fission track thermochronometry. *Tectonics* 32, 1513–1528. doi:10.1002/tect.20082
- Feinstein, S., Kohn, B. P., Steckler, M. S., and Eyal, M. (1996). Thermal history of the eastern margin of the Gulf of Suez, I. reconstruction from borehole temperature and organic maturity measurements. *Tectonophysics* 266, 203–220. doi:10.1016/S0040-1951(96)00190-4
- Fritz, H., Abdelsalam, M., Ali, K. A., Bingen, B., Collins, A. S., Fowler, A. R., et al. (2013). Orogen styles in Israel and its implications for the neoproterozoic to cambrian tectonic evolution. *J. Afr. Earth Sci.* 86, 65–106. doi:10.1016/j.jafrearsci.2013.06.004
- Garfunkel, Z., and Derin, B. (1985). “Permian-Early Mesozoic tectonism and continental margin formation in Israel and its implications for the history of the Eastern Mediterranean,” in *The geological evolution of the eastern Mediterranean*. Editors J. E. Dixon and A. H. F. Robertson (Oxford: Blackwell), 187–201.
- Garfunkel, Z. (1988). Relation between continental rifting and uplifting – evidence from the Suez Rift and northern Red-Sea. *Tectonophysics* 150, 33–49. doi:10.1016/0040-1951(88)90294-6
- Garver, J. I. (2003). Etching zircon age standards for fission-track analysis. *Radiat. Meas.* 37, 47–53. doi:10.1016/S1350-4487(02)00127-0
- George, R., Rogers, N., and Kelley, S. (1998). Earliest magmatism in Ethiopia: Evidence for two mantle plumes in one flood basalt province. *Geol* 26, 923. doi:10.1130/0091-7613(1998)026<0923:EMIEEF>2.3.CO;2
- Ghebreab, W., Carter, A., Hurford, A. J., and Talbot, C. J. (2002). Constraints for timing of extensional tectonics in the Western margin of the Red Sea in Eritrea. *Earth Planet. Sci. Lett.* 1 (2), 107–119. doi:10.1016/S0012-821X(02)00621-0
- Girdler, R. W. (1985). Problems concerning the evolution of oceanic lithosphere in the northern Red Sea. *Tectonophysics* 116, 109–122. doi:10.1016/0040-1951(85)90224-0
- Gleadow, A. J. W., and Duddy, I. R. (1981). A natural long-term track annealing experiment for apatite. *Nucl. Tracks* 5, 169–174. doi:10.1016/0191-278X(81)90039-1
- Gleadow, A. J. W., Duddy, I. R., Green, P. F., and Lovering, J. F. (1986). Confined fission track lengths in apatite: A diagnostic tool for thermal history analysis. *Contributions Mineralogy Petrology* 94, 405–415. doi:10.1007/BF00376334
- Gleadow, A. J. W., Duddy, I. R., and Lovering, J. F. (1983). Fission track analysis: A new tool for the evaluation of thermal histories and hydrocarbon potential. *APPEA J.* 23, 93. doi:10.1071/AJ82009
- Green, P. F., Duddy, I. R., Laslett, G. M., Hegarty, K. A., Gleadow, A. J. W., and Lovering, J. F. (1989). Thermal annealing of fission track in apatite: 4 quantitative modelling techniques and extension to geological time scales. *Chem. Geol.* 79, 155–182. doi:10.1016/0168-9622(89)90018-3
- Greiling, R. O., Kriiner, A., El Ramly, M. F., and Rashwan, A. A. (1988). “Structural relationships between the southern and central parts of the Eastern Desert of Egypt: Details of a fold and thrust belt.” in *The pan-african of NE Africa and adjacent areas*. Editors S. El Gaby and R. O. Greiling (Wiesbaden: Vieweg), 121–145.
- Grobe, A., von Hagke, C., Littke, R., Dunkl, I., Wübbeler, F., Muecher, P., et al. (2019). Tectono-thermal evolution of Oman’s mesozoic passive continental margin under the obducting seamount ophiolite: A case study of jebel akhdar, Oman. *Solid earth.* 10, 149–175. doi:10.5194/se-10-149-2019
- Gvrtzman, G., and Weissbrod, T. (1984). The hercynian geanticline of helez and the late palaeozoic history of the levant. *Geol. Soc. Lond. Spec. Publ.* 17, 177–186. doi:10.1144/GSL.SP.1984.017.01.11
- Hansen, S. E., Nyblade, A. A., and Benoit, M. H. (2012). Mantle structure beneath Africa and Arabia from adaptively parameterized P-wave tomography: Implications for the origin of Cenozoic Afro-Arabian tectonism. *Earth Planet. Sci. Lett.* 319–320, 23–34. doi:10.1016/j.epsl.2011.12.023
- Hasebe, N., Barbarand, J., Jarvis, K., Carter, A., and Hurford, A. J. (2004). Apatite fission-track chronometry using laser ablation ICP-MS. *Chem. Geol.* 207, 135–145. doi:10.1016/j.chemgeo.2004.01.007
- Hashad, A. H. (1978). Present status of geochronological data on the Egyptian basement complex. *Precambrian Res.* 6, A24–A25. doi:10.1016/0301-9268(78)90094-3
- Hassan, A. A. (1967). A new carboniferous occurrence in Abu durba, Sinai, Egypt. *Proc. 6th Arab Petroleum Congr. Baghdad* 2, 1–8.
- Hofmann, C., Courtillot, V., Féraud, G., Rochette, P., Yirgu, G., Ketefo, E., et al. (1997). Timing of the Ethiopian flood basalt event and implications for plume birth and global change. *Nature* 389, 838–841. doi:10.1038/39853

- Hughes, G. W., Varol, O., and Beydoun, Z. R. (1991). Evidence for middle Oligocene rifting of the Gulf of Aden and for late Oligocene rifting of the southern Red Sea. *Mar. Petroleum Geol.* 8, 354–358. doi:10.1016/0264-8172(91)90088-1
- Hurford, A. J. (1990). Standardization of fission track dating calibration: Recommendation by the fission track working group of the I.U.G.S. Subcommittee on geochronology. *Chem. Geol.* 80, 171–178. doi:10.1016/0168-9622(90)90025-8
- Johnson, P. R. (2014). An expanding arabian-nubian shield geochronologic and isotopic dataset: Defining limits and confirming the tectonic setting of a neoproterozoic accretionary orogen. *Open Geol. J.* 8, 3–33. doi:10.2174/1874262901408010003
- Johnson, P. R., Andresen, A., Collins, A. S., Fowler, A. R., Fritz, H., Ghebreab, W., et al. (2011). Late cryogenian–ediacaran history of the arabian–nubian shield: A review of depositional, plutonic, structural, and tectonic events in the closing stages of the northern East African orogen. *J. Afr. Earth Sci.* 61, 167–232. doi:10.1016/j.jafrearsci.2011.07.003
- Kassem, A., Sharaf, L., Baghdady, A., and Abd El-Naby, A. (2020). Cenomanian/Turonian oceanic anoxic event 2 in October oil field, central Gulf of Suez, Egypt. *J. Afr. Earth Sci.* 165, 103817. doi:10.1016/j.jafrearsci.2020.103817
- Ketcham, R. A., Donelick, R. A., Balestrieri, M. L., and Zattin, M. (2009). Reproducibility of apatite fission-track length data and thermal history reconstruction. *Earth Planet. Sci. Lett.* 284, 504–515. doi:10.1016/j.epsl.2009.05.015
- Ketcham, R. A. (2005). Forward and inverse modeling of low-temperature thermochronometry data. *Rev. Mineralogy Geochem.* 58, 275–314. doi:10.2138/rmg.2005.58.11
- Ketcham, R. A. (2009). HeFTy, version 1.6.7.
- Klitzsch, E. (1990). “Paleozoic,” in *The Geology of Egypt*. Editor R. Said (Balkema, Rotterdam: Brookfield), 451–486.
- Klitzsch, E. (1986). Plate tectonics and cratonal geology in Northeast Africa (Egypt, Sudan). *Geol. Rundsch.* 75, 755–768. doi:10.1007/BF01820645
- Klitzsch, E., and Wycisk, P. (1987). Geology of the sedimentary basins of northern Sudan and bordering areas. *Berl. Geowiss. Abh. Reihe A Geol. Palaeontologie* 75, 97–136.
- Kohn, B. P., Eyal, M., and Feinstein, S. (1992). A major late devonian-early carboniferous (hercynian) thermotectonic event at the NW margin of the arabian-nubian shield: Evidence from zircon fission track dating. *Tectonics* 11, 1018–1027. doi:10.1029/92TC00636
- Kohn, B. P., and Eyal, M. (1981). History of uplift of the crystalline basement of Sinai and its relation to opening of the Red Sea as revealed by fission track dating of apatites. *Earth Planet. Sci. Lett.* 52, 129–141. doi:10.1016/0012-821X(81)90215-6
- Kohn, B. P., Feinstein, S., Foster, D. A., Steckler, M. S., and Eyal, M. (1997). Thermal history of the eastern Gulf of Suez, II. Reconstruction from apatite fission track and K-feldspar measurements. *Tectonophysics* 283, 219–239. doi:10.1016/S0040-1951(97)00069-3
- Kohn, B., Weissbrod, T., Chung, L., Farley, K., and Bodorkos, S. (2019). Low-temperature thermochronology of francolite: Insights into timing of Dead Sea Transform motion. *Terra nova*. 31, 205–219. doi:10.1111/ter.12387
- Kolodner, K., Avigad, D., McWILLIAMS, M., Wooden, J. L., Weissbrod, T., and Feinstein, S. (2006). Provenance of north Gondwana cambrian–ordovician sandstone: U–Pb SHRIMP dating of detrital zircons from Israel and Jordan. *Geol. Mag.* 143, 367–391. doi:10.1017/S0016756805001640
- Kora, M. (1984). *The paleozoic outcrops of Um Bogma area*. Sinai: AAPG Bulletin.
- Kröner, A., Kruger, J., and Rashwan, A. A. A. (1994). Age and tectonic setting of granitoid gneisses in the Eastern Desert of Egypt and south-west Sinai. *Geol. Rundsch* 83, 502–513. doi:10.1007/bf01083223
- Lambiase, J. J., and Morley, C. K. (1999). Hydrocarbons in rift basins: The role of stratigraphy. *Philosophical Trans. R. Soc. Lond.* 357, 877–900. doi:10.1098/rsta.1999.0356
- Leroy, S., d’Acremont, E., Tiberi, C., Basuyau, C., Autin, J., Lucazeau, F., et al. (2010). Recent off-axis volcanism in the eastern Gulf of Aden: Implications for plume–ridge interaction. *Earth Planet. Sci. Lett.* 293, 140–153. doi:10.1016/j.epsl.2010.02.036
- Leroy, S., Razin, P., Autin, J., Bache, F., d’Acremont, E., Watremez, L., et al. (2012). From rifting to oceanic spreading in the Gulf of Aden: A synthesis. *Arab. J. Geosci.* 5, 859–901. doi:10.1007/s12517-011-0475-4
- Li, J., Zhang, Z., Zhao, Y., Pei, J., Tang, W., and Li, K. (2017). Detrital apatite fission track analyses of the subei basin: Implications for basin-range structure of the northern Tibetan plateau. *Int. Geol. Rev.* 59 (2), 204–218. doi:10.1080/00206814.2016.1219880
- Lisker, F., Ventura, B., and Glasmacher, U. A. (2009). Apatite thermochronology in modern geology. *Geol. Soc. Lond. Spec. Publ.* 324, 1–23. doi:10.1144/SP324.1
- Longerich, H. P., Jackson, S. E., and Günther, D. (1996). Inter-laboratory note. Laser ablation inductively coupled plasma mass spectrometric transient signal data acquisition and analyte concentration calculation. *J. Anal. At. Spectrom.* 11, 899–904. doi:10.1039/JA9961100899
- Mansour, S. E. E. (2016). Long-term topographic evolution of the African plate, causes and consequences for surrounding lithospheric plates. Ph.D. Thesis. Heidelberg, Germany: Universität Heidelberg, 277. doi:10.11588/heidok.00020122
- Mansour, S., Glasmacher, U. A., Krob, F. C., Casillas, R., and Albinger, M. (2022b). Timing of rapid cooling and erosional decay of two volcanic islands of the canary archipelago: Implications from low-temperature thermochronology. *Int. J. Earth Sci.* 112 (1), 345–382. doi:10.1007/s00531-022-02253-7
- Mansour, S., Hasebe, N., Abdelrahman, K., Fnais, M. S., and Tamura, A. (2023b). Reconstructing the tectonic history of the arabian–nubian shield in Sinai: Low-temperature thermochronology implications on Wadi agar area. *Minerals* 13, 574. doi:10.3390/min13040574
- Mansour, S., Hasebe, N., Azab, E., Elnaggar, A. Y., and Tamura, A. (2021). Combined zircon/apatite U–Pb and fission-track dating by LA-ICP-MS and its geological applications: An example from the Egyptian younger granites. *Minerals* 11, 1341. doi:10.3390/min11121341
- Mansour, S., Hasebe, N., Meert, J. G., Tamura, A., Khalaf, F. I., and El-Shafei, M. K. (2022a). Evolution of the arabian-nubian shield in gabal samra area, Sinai; implications from zircon U–Pb geochronology. *J. Afr. Earth Sci.* 192, 104538. doi:10.1016/j.jafrearsci.2022.104538
- Mansour, S., Hasebe, N., and Tamura, A. (2023a). Erosional reservoir for the northern segment of the arabian-nubian shield: Constrains from U–Pb geochronology of the lower palaeozoic succession, North Eastern Desert, Egypt. *Precambrian Res.* 388, 107017. doi:10.1016/j.precamres.2023.107017
- McClay, K. R., Nichols, G. J., Khalil, S. M., Darwish, M., and Bosworth, W. (1998). “Extensional tectonics and sedimentation, eastern Gulf of Suez, Egypt,” in *Sedimentation and tectonics in rift basins Red Sea- Gulf of Aden*. Editors B. H. Purser and D. W. J. Bosence (Dordrecht: Springer Netherlands), 223–238. doi:10.1007/978-94-011-4930-3_14
- McWilliams, M. O. (1981). “Chapter 26 palaeomagnetism and precambrian tectonic evolution of Gondwana,” in *Developments in precambrian Geology* (Elsevier), 649–687. doi:10.1016/S0166-2635(08)70031-8
- Meert, J. G., Pandit, M. K., Pradhan, V. R., and Kamenov, G. (2011). Preliminary report on the paleomagnetism of 1.88Ga dykes from the Bastar and Dharwar cratons, Peninsular India. *Gondwana Res.* 20, 335–343. doi:10.1016/j.gr.2011.03.005
- Meneisy, M. Y. (1986). *Mesozoic igneous activity in Egypt*. Doha, Qatar: Qatar University.
- Menzies, M., Gallagher, K., Yelland, A., and Hurford, A. J. (1997). Volcanic and nonvolcanic rifted margins of the Red Sea and Gulf of Aden: Crustal cooling and margin evolution in Yemen. *Geochimica Cosmochimica Acta* 61, 2511–2527. doi:10.1016/S0016-7037(97)00108-7
- Morag, N., Haviv, I., Eyal, M., Kohn, B. P., and Feinstein, S. (2019). Early flank uplift along the Suez Rift: Implications for the role of mantle plumes and the onset of the Dead Sea Transform. *Earth Planet. Sci. Lett.* 516, 56–65. doi:10.1016/j.epsl.2019.03.002
- Morgan, P., Boulos, F. K., Hennin, S. F., El-Sherif, A. A., El-Sayed, A. A., Basta, N. Z., et al. (1985). Heat flow in Eastern Egypt: The thermal signature of a continental breakup. *J. Geodyn.* 4, 107–131. doi:10.1016/0264-3707(85)90055-9
- Morley, C. K. (1999). *Geoscience of rift systems—evolution of East Africa*. Tulsa, United States: AAPG, 44.
- Mount, V. S., Crawford, R. I. S., and Bergman, S. C. (1998). Regional structural style of the central and southern Oman mountains: Jebel akhdar, saih hatat, and the northern ghaba basin. *GeoArabia* 3, 475–490. doi:10.2113/geoarabia0304475
- Moustafa, A. R., and Fouda, H. G. A. (2014). Structural architecture and tectonic evolution of the Yelleg inverted half graben, northern Sinai, Egypt. *Mar. Petroleum Geol.* 51, 286–297. doi:10.1016/j.marpetgeo.2014.01.001
- Moustafa, A. R., and Yousif, M. S. M. (1993). Structural evolution of the eastern shoulder of the Suez Rift: Um Bogma area. *Neues Jahrb. für Geol. Paläontologie - Monatsh.* 1993, 655–668. doi:10.1127/njgpm/1993/1993/655
- Naeser, C. W., and Faul, H. (1969). Fission track annealing in apatite and sphene. *J. Geophys. Res.* 74/2, 705–710. doi:10.1029/jb074i002p00705
- Naylor, D., Al-Rawi, M., Clayton, G., Fitzpatrick, M. J., and Green, P. F. (2013). Hydrocarbon potential in Jordan. *J. Petroleum Geol.* 36, 205–236. doi:10.1111/jpg.12553
- Nonn, C., Leroy, S., Lescanne, M., and Castilla, R. (2019). Central Gulf of Aden conjugate margins (Yemen-Somalia): Tectono-sedimentary and magmatism evolution in hybrid-type margins. *Mar. Petroleum Geol.* 105, 100–123. doi:10.1016/j.MARPETGEO.2018.11.053
- Nuriel, P., Weinberger, R., Kylander-Clark, A. R. C., Hacker, B. R., and Craddock, J. P. (2017). The onset of the Dead Sea transform based on calcite age-strain analyses. *Geology* 45 (7), 587–590. doi:10.1130/G38903.1
- Omar, G. I., Kohn, B. P., Lutz, T. M., and Faul, H. (1987). The cooling history of Silurian to Cretaceous alkaline ring complexes, south Eastern Desert, Egypt, as revealed by fission-track analysis. *Earth Planet. Sci. Lett.* 83, 94–108. doi:10.1016/0012-821X(87)90054-9
- Omar, G. I., Steckler, M. S., Buck, W. R., and Kohn, B. P. (1989). Fission-track analysis of basement apatites at the Western margin of the Gulf of Suez rift, Egypt: Evidence for synchronicity of uplift and subsidence. *Earth Planet. Sci. Lett.* 94, 316–328. doi:10.1016/0012-821X(89)90149-0
- Omar, G. I., and Steckler, M. S. (1995). Fission track evidence on the initial rifting of the Red Sea: Two pulses, No propagation. *Science* 270, 1341–1344. doi:10.1126/science.270.5240.1341
- Osman, A. (1954). Upper cretaceous foraminifera of western Sinai. *Fac. Eng. Bull. Cairo Univ.* Cairo, Egypt: Cairo University 26, 335–365.

- Pearce, N. J. G., Perkins, W. T., Westgate, J. A., Gorton, M. P., Jackson, S. E., Neal, C. R., et al. (1997). A compilation of new and published major and trace element data for NIST SRM 610 and NIST SRM 612 glass reference materials. *Geostand. Geoanalytical Res.* 21, 115–144. doi:10.1111/j.1751-908X.1997.tb00538.x
- Pik, R., Bellahsen, N., Leroy, S., Denèle, Y., Razin, P., Ahmed, A., et al. (2013). Structural control of basement denudation during rifting revealed by low-temperature (U–Th–Sm)/He thermochronology of the socotra island basement—southern Gulf of aden margin. *Tectonophysics* 607, 17–31. doi:10.1016/j.tecto.2013.07.038
- Platt, J. P., and England, P. C. (1993). Convective removal of lithosphere beneath mountain belts: Thermal and mechanical consequences. *Am. J. Sci.* 293, 307–336. doi:10.2475/ajs.294.3.307
- Refaat, A. A., and Imam, M. M. (1999). The Tayiba red beds: Transitional marine-continental deposits in the precursor Suez Rift, Sinai, Egypt. *J. Afr. Earth Sci.* 26, 487–506. doi:10.1016/S0899-5362(99)00029-9
- Reiners, P. W., and Ehlers, T. A. (2005). in *Low-temperature thermochronology: Techniques, interpretations, and applications* (Chantilly, Va: Mineralogical Society of America).
- Rooney, T. O. (2017). The cenozoic magmatism of East-Africa: Part I — flood basalts and pulsed magmatism. *Lithos* 286–287, 264–301. doi:10.1016/j.lithos.2017.05.014
- Said, R. (1971). *Explanatory notes to accompany the geological map of Egypt*. Cairo, Egypt: The Egyptian Geological Survey.
- Said, R. (1962). *The Geology of Egypt*. 1st ed Netherlands: Elsevier, Amsterdam.
- Said, R. (1990). *The Geology of Egypt*. 2nd ed Netherlands: A.A. Balkema, Rotterdam.
- Sallam, E. S., Afife, M. M., Fares, M., van Loon, A. J., and Ruban, D. A. (2019). Sedimentary facies and diagenesis of the Lower Miocene Rudeis Formation (southwestern offshore margin of the Gulf of Suez, Egypt) and implications for its reservoir quality. *Mar. Geol.* 413, 48–70. doi:10.1016/j.margeo.2019.04.004
- Seilacher, A. (1990). “Paleozoic trace fossils,” in *Geology of Egypt* (Netherlands, Rotterdam: Routledge), 113–156.
- Sengör, A. M. C., and Burke, K. (1978). Relative timing of rifting and volcanism on Earth and its tectonic implications. *Geophys. Res. Lett.* 5, 419–421. doi:10.1029/GL005i006p00419
- Serra-Kiel, J., Gallardo-García, A., Razin, Ph., Robinet, J., Roger, J., Grelaud, C., et al. (2016). Middle eocene-early Miocene larger foraminifera from dhofar (Oman) and socotra island (Yemen). *Arab. J. Geosci.* 9, 344. doi:10.1007/s12517-015-2243-3
- Sestini, G. (1984). Tectonic and sedimentary history of the NE african margin (Egypt—Libya). *Geol. Soc. Lond. Spec. Publ.* 17, 161–175. doi:10.1144/GSL.SP.1984.017.01.10
- Shalaby, A. (2017). Fracture patterns of the drainage basin of Wadi Dahab in relation to tectonic-landscape evolution of the Gulf of Aqaba - Dead Sea transform fault. *J. Asian Earth Sci.* 148, 192–209. doi:10.1016/j.jseae.2017.08.035
- Shalaby, A., and Shawky, M. (2014). Morphotectonics of kid drainage basin, southeastern Sinai: A landscape evolution coeval to Gulf of aqaba - Dead Sea rifting. *J. Afr. Earth Sci.* 100, 289–302. doi:10.1016/j.jafrearsci.2014.06.025
- Shehata, A. A., El Fawal, F. M., Ito, M., Aboulmagd, M. A., and Brooks, H. L. (2020). Senonian platform-to-slope evolution in the tectonically-influenced Syrian Arc sedimentary belt: Beni Suef Basin, Egypt. *J. Afr. Earth Sci.* 170, 103934. doi:10.1016/j.jafrearsci.2020.103934
- Shehata, A. A., Sarhan, M. A., Abdel-Fattah, M. I., and Mansour, S. (2023). Geophysical assessment for the oil potentiality of the Abu roash “G” reservoir in west beni suef basin, western Desert, Egypt. *J. Afr. Earth Sci.* 199, 104845. doi:10.1016/j.jafrearsci.2023.104845
- Stab, M., Bellahsen, N., Pik, R., Quidelleur, X., Ayalew, D., and Leroy, S. (2016). Modes of rifting in magma-rich settings: Tectono-magmatic evolution of central Afar: Modes of rifting in magma-rich settings. *Tectonics* 35, 2–38. doi:10.1002/2015TC003893
- Stampfii, G. M., von Raumer, J. F., and Borel, G. D. (2002). “Paleozoic evolution of pre-Variscan terranes: From Gondwana to the Variscan collision,” in *Variscan-Appalachian dynamics: The building of the late Paleozoic basement* (Boulder, USA: Geological Society of America). doi:10.1130/0-8137-2364-7.263
- Steckler, M. S. (1985). Uplift and extension at the Gulf of Suez: Indications of induced mantle convection. *Nature* 317, 135–139. doi:10.1038/317135a0
- Stern, R. J. (1994). ARC assembly and continental collision in the neoproterozoic East African orogen: Implications for the consolidation of gondwanaland. *Annu. Rev. Earth Planet. Sci.* 22, 319–351. doi:10.1146/annurev.ea.22.050194.001535
- Stern, R. J., and Hedge, C. E. (1985). Geochronologic and isotopic constraints on late Precambrian crustal evolution in the Eastern Desert of Egypt. *Am. J. Sci.* 285, 97–127. doi:10.2475/ajs.285.2.97
- Sultan, I. Z. (1985). On the presence of middle jurassic miospores at gebel el iseila, west central Sinai, Egypt. *Bull. Fac. Sci.* 25, 26–40.
- Szymanski, E., Stockli, D. F., Johnson, P. R., and Hager, C. (2016). Thermochronometric evidence for diffuse extension and two-phase rifting within the central arabian margin of the red Sea Rift. *Tectonics* 35, 2863–2895. doi:10.1002/2016TC004336
- Tewfik, N., Harwood, C., and Deighton, I. (1992). Miocene, Rudeis and Kareem formations in the Gulf of Suez: Aspects of sedimentology and geochemistry. *EGPC Explor. Semin.* 11, 84–113.
- Vermeesch, P., Avigad, D., and McWilliams, M. O. (2009). 500 m.y. of thermal history elucidated by multi-method detrital thermochronology of North Gondwana Cambrian sandstone (Eilat area, Israel). *GSA Bull.* 121, 1204–1216. doi:10.1130/B26473.1
- Vermeesch, P. (2018). IsoplotR: A free and open toolbox for geochronology. *Geosci. Front.* 9, 1479–1493. doi:10.1016/j.gsf.2018.04.001
- Wagner, G. A. (1972). Spaltspurenalter von Mineralen und natürlichen gläsern: Eine übersicht. *Fortschritte Mineral.* 1972, 114–145.
- Walder, A. J., Platzner, I., and Freedman, P. A. (1993). Isotope ratio measurement of lead, neodymium and neodymium–samarium mixtures, Hafnium and Hafnium–Lutetium mixtures with a double focusing multiple collector inductively coupled plasma mass spectrometer. *J. Anal. At. Spectrom.* 8, 19–23. doi:10.1039/JA9930800019
- Weissbrod, T. (1969). The Paleozoic of Israel and Adjacent countries. Pt 1: The subsurfacealeozoic stratigraphy of southern Israel. *Isr. Geol. Surv. Bull.* 47, 35.
- Willis, K. M., Stern, R. J., and Clauer, N. (1988). Age and geochemistry of Late Precambrian sediments of the Hammamat series from the Northeastern Desert of Egypt. *Precambrian Res.* 42, 173–187.
- Yamada, R., Tagami, T., Nishimura, S., and Ito, H. (1995). Annealing kinetics of fission tracks in zircon: An experimental study. *Chem. Geol.* 122, 249–258. doi:10.1016/0009-2541(95)00006-8
- Zheng, D., Zhang, P., and Wan, J. (2003). Late cenozoic deformation subsequence in northeastern margin of tibet —detrital AFT records from linxia basin. *Sci. China Ser. D Earth Sci.* 46 (2), 266–275. doi:10.1360/03dz0021